Large-eddy simulation of gas turbine combustors

By Krishnan Mahesh †, George Constantinescu, Sourabh Apte, Gianluca Iaccarino AND Parviz Moin

1. Motivation and objectives

This report discusses our progress towards developing a numerical algorithm, and solver capable of performing large-eddy simulation in geometries as complex as the combustor of a gas-turbine engine. LES is considered a particularly attractive approach for combustor simulation because of its demonstrated superiority over RANS in predicting mixing. A working combustor – the PW6000 – is chosen to develop and demonstrate LES capability.

As discussed in previous reports (Mahesh *et al.* 1999, 2000), an algorithm and LES solver for unstructured grids are under development.

2. Accomplishments

Our progress in the last year is as follows:

• A new formulation was derived that is discretely energy-conserving for arbitrary grids. This was found essential to perform simulations at high Reynolds numbers, and on 'bad' grids encountered in complex geometries such as the Pratt & Whitney combustor.

• Turbulent validations were performed for the swirling flow in a coaxial combustor geometry, flow over a cylinder and turbulent channel flow.

• Turbulent simulations were initiated in the complex Pratt & Whitney combustor. Also simulations were performed in a test rig geometry used by Pratt & Whitney for which experimental data is available.

• A spray module was integrated with the gas-phase solver. Validation simulations in a swiring coaxial combustor geometry Sommerfeld & Qiu (1991) were performed. Spray simulations in the Pratt & Whitney combustor were initiated.

3. Algorithm improvements

3.1. *Base algorithm*

Recall that the algorithm described at the end of last year's report stored pressure at the centroids of the elements, and velocity at their faces. As shown in figure 1, only the normal component of velocity was stored and advanced in time; the other two components were reconstructed. The velocity component v_n satisfied,

$$\frac{\partial v_n}{\partial t} - (\vec{u} \times \vec{\omega}) \cdot \vec{n} + \frac{\partial}{\partial n}\left(\frac{\vec{u} \cdot \vec{u}}{2}\right) = -\frac{1}{\rho}\frac{\partial p}{\partial n} + \nu \left(\nabla^2 \vec{u}\right) \cdot \vec{n}. \tag{3.1}$$

The convection term was written in terms of velocity and vorticity, and the pressure-projection approach was used to ensure that the velocity field was discretely divergence-free. As shown in last year's report, good results were obtained for laminar unsteady flows, and low Reynolds number turbulent flows in complex geometries.

† Aerospace Engineering and Mechanics, University of Minnesota

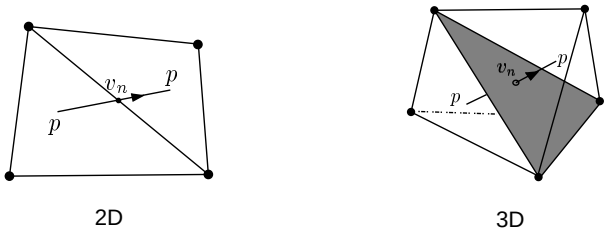

FIGURE 1. Positioning of variables in staggered algorithm.

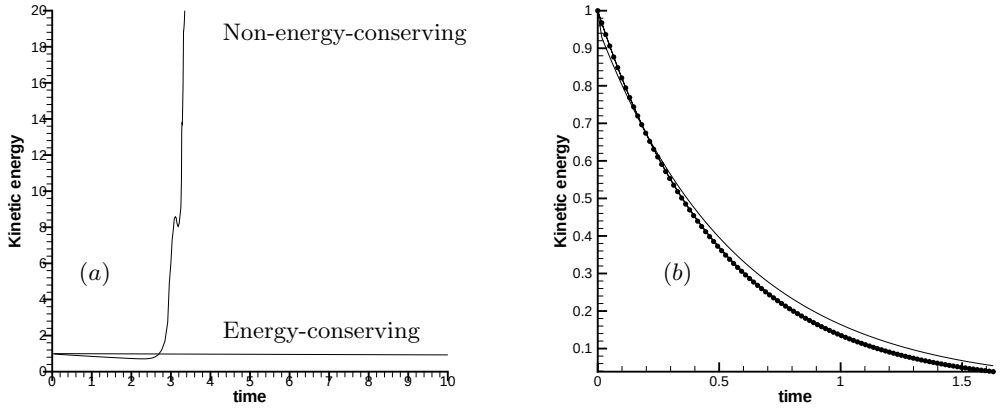

FIGURE 2. Illustration of the importance of discretely conserving kinetic energy. The kinetic energy is plotted against time for the Taylor problem at (a): $Re = 10^9$, and (b): $Re = 1$. At the lower Reynolds number, both schemes are stable. At higher Reynolds number, only the energy-conserving scheme is stable. The solid circles in (b) denote the analytical solution; the energy-conserving formulation passes through them.

However, problems with robustness were experienced this year when the simulations were extended to high Reynolds number, and to 'bad' grid elements that are inevitable in complex geometries such as the combustor geometry provided by Pratt & Whitney. It was established that the robustness problems were caused by the fact that the algorithm only conserved momentum, and not kinetic energy, on arbitrary grids with highly skewed elements.

An alternative formulation was derived, in which the convection term discretely conserves kinetic energy for arbitrary grids. Recall that discrete energy conservation refers to the fact that for incompressible flow, the convection term in the kinetic energy equation is expressible in divergence form, i.e. $\partial/\partial x_j\,(u_j u_i u_i/2)$. Conservation of momentum and the continuity equation ensure kinetic energy conservation for the continuous equations; however the same is not true for the discrete equations, where momentum conservation does not imply energy conservation. It is readily seen that kinetic energy conservation is a desirable feature for the algorithm since it implies that the L_2 norm is bounded.

The basic idea behind the new formulation is as follows. The traditional fractional-step algorithm on structured grids stores the face-normal velocity component on all faces. Control volumes are then identified around the faces, and the momentum equation for the velocity component is advanced in time. The primary reason for staggering is that

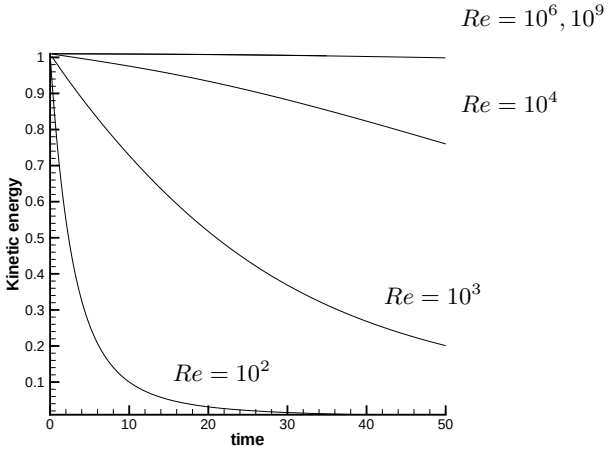

FIGURE 3. Kinetic energy of isotropic turbulence is plotted against time at varying Reynolds numbers. The Reynolds number is increased from $10^2, 10^3, 10^4, 10^6$ and 10^9 respectively. Note that the scheme is robust even at the highest Reynolds numbers.

the pressure equation does not suffer from odd-even decoupling. However, solution of the momentum equation requires that the velocity components tangential to the face be known. These are obtained through interpolation. The interpolant has to be carefully constructed such that the resulting momentum equation implies conservation of kinetic energy. There are two problems with extending this approach to arbitrary unstructured grids: (i) defining control volumes around the faces in three-dimensions is complicated; furthermore, skewed elements yield highly skewed control volumes. (ii) the resulting interpolation for the tangential velocities is unacceptably inaccurate if discrete energy conservation is required. We base these statements on actual computations performed using an energy-conserving formulation that we derived from a fully staggered formulation. The resulting formulation yielded acceptable results for Cartesian grids but was unacceptably inaccurate for the complex Pratt & Whitney combustor geometry.

An alternative formulation was therefore derived. Velocity and pressure are now stored at the centroids of the *volumes*. The cell-centered velocities are advanced in the predictor step such that kinetic energy conservation is ensured for the predictor step. These predicted velocities are then interpolated to the faces and then projected. Both interpolation and projection are robust procedures since they do not add energy to the solution (when the computational stencil uses local neighbors). Projection yields the pressure potential at the cell-centers, and the pressure gradient is used to correct the cell velocities. A straightforward use of the gradient theorem yields very good results on smooth grids, but is found unacceptable for highly skewed or very rapidly varying grids. This lack of robustness can be explained from an energy-conservation point of view. A novel discretization for the pressure gradient was derived. This formulation of the algorithm has been found to yield very good results for both 'simple' problems (Taylor problem, isotropic turbulence, channel, cylinder, coaxial combustor) as well as the exceedingly complex geometry of the Pratt & Whitney combustor.

The importance of discrete energy conservation is illustrated in Fig. 2, which shows the evolution of kinetic energy in the Taylor problem – an analytical solution, which describes counter-rotating vortices that decay in time. Our energy-conserving formulation is com-

Gas Phase (Air)		*Particle Phase (Glass)*	
Flow rate in primary jet, g/s	9.9	Loading Ratio in Primary Jet	0.034
Flow rate in secondary jet, g/s	38.3	Flow rate, g/s	0.34
Inlet Reynolds number	26200	Density ratio, ρ_p/ρ_f	2152
Swirl number	0.47		

TABLE 1. Flow conditions and particle properties used in the Sommerfeld & Qiu (1991) experiments.

pared to a non-dissipative formulation that only conserves momentum. Both formulations have the same computational stencil. At low Reynolds numbers, where the dissipative scales are resolved, both formulations are stable, although the energy-conserving formulation shows better agreement with the analytical result. However, at very high Reynolds numbers where the dissipative scales are not resolved, the formulation that does not conserve kinetic energy becomes unstable after some time, while the energy conserving formulation is seen to maintain its initial kinetic energy as required by the analytical solution. Figure 3 shows the decay of turbulent kinetic energy of isotropic turbulence when computed on a coarse grid (32^3). The Reynolds number is increased from 100 to 10^9. No subgrid model is used. Even the lowest Reynolds number is not completely resolved at this resolution. Note however that the solution does not become numerically unstable; instead it exhibits the proper Reynolds number sensitivity (reduced decay rate with increasing Reynolds number). It is this robustness that makes accurate LES of high Reynolds number flows possible.

3.2. *Integration with spray modules*

The gas-phase solver was extended to include the effect of liquid droplets. The droplets are modeled as point particles which satisfy Lagrangian equations. They influence the gas phase through source terms in the gas-phase equations. As the particles move, their position is located and each particle is assigned to a control volume of the gas-phase grid. The gas-phase properties are interpolated to the particle location and the particle equations are solved. The particles are then relocated, particles that cross interprocessor boundaries in our parallel computaton are duly transferred, source terms in the gas-phase equation are computed, and the computation is further advanced. Spray integration involves the following key issues: (i) Efficient search and location of droplets on an unstructured grid (ii) Interpolation of gas-phase properties to the droplet location for arbitrarily shaped control volumes (iii) inter-processor droplet transfer.

3.2.1. *Locating particles in elements of arbitrary shape*

Locating particles in a generalized-coordinate structured code is straightforward, since the physical coordinates can be transformed into a uniform computational space. However, this is not the case for unstructured grids. Westermann (1992) describes several

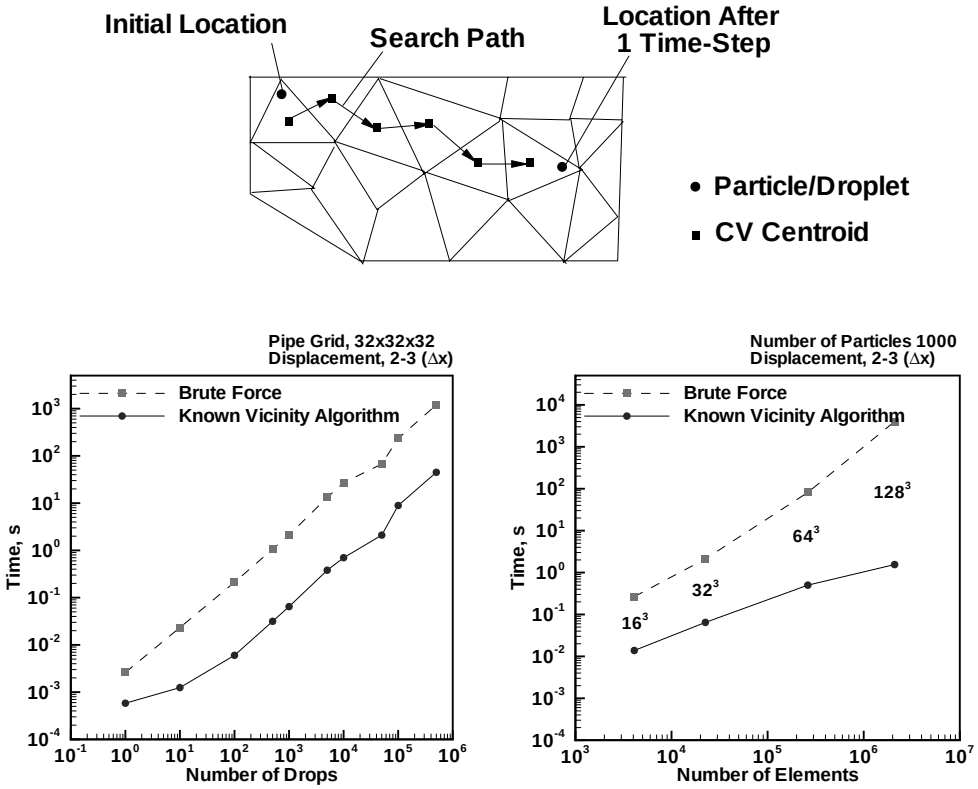

FIGURE 4. (*a*) Schematic of the known-vicinity algorithm to track particle positions on unstructured grids. (*b*) Comparison of the brute force and known vicinity search algorithms.

approaches to locate particles in particle-in-cell codes. Two such techniques are implemented in the unstructured code, and are described below.

One approach to determining whether a particle lies inside a control volume is based on the calculation of partial volumes. The nodes of the control volume are joined to the particle location, and the volumes of the resulting sub-cells are compared to that of the control volume. If the particle lies inside the control volume, the sum of the sub-cell volumes will be equal to the total volume. The advantage of this method is that it can be applied to all control volumes simultaneously and a separate search algorithm for particle location is not required. However, the method is slow since it involves computations of partial volumes for each cell. Also, it was found to fail drastically for highly skewed meshes due to inaccuracies in the computation of partial volumes.

The second approach projects the particle location onto the faces of the control volume and compares these vectors with outward face-normals for all faces. If the particle lies within the cell, the projected vectors point the same way as the outward face-normals. This technique, although more accurate, requires a search algorithm to select the control volume to which the criterion is applied.

3.2.2. *Search algorithms for particles on unstructured grids*

Three approaches were examined and are termed the brute-force, modified-brute-force and known-vicinity approaches respectively. The brute-force approach simply loops over

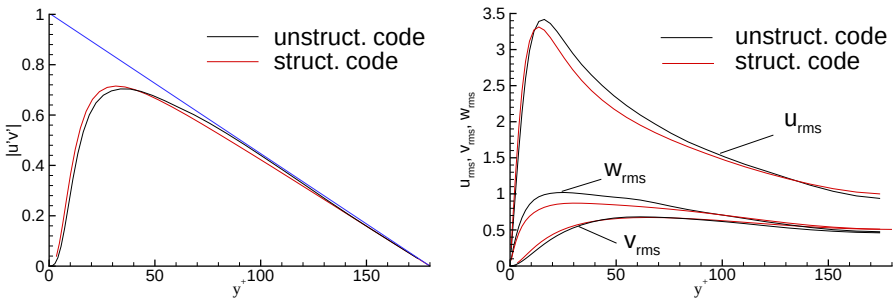

FIGURE 5. Comparison of the unstructured solver to a structured solver using the same grid. Results correspond to turbulent Reynolds stresses in a turbulent channel at $Re_\tau = 180$ on a coarse $(32 \times 64 \times 32)$ grid. The structured grid results were kindly provided by Dr. Bill Cabot, Lawrence Livermore National Laboratory.

all the elements of the grid and applies the localization criterion described above. As expected, it is extremely slow when particles number about a million, as is the case even for coarse LES. The modified-brute-force approach evaluates the closest point of the mesh to the particle location and only considers the elements surrounding that point. Should this attempt (which in general is very successful) fail, the elements surrounding all the close points are considered. If this also fails for some pathological cases Lohner (1995), the search region is enlarged or the brute-force method is applied. This modified approach is found effective to initialize particles, and as a fall-back position for more refined algorithms.

Given a good initial guess for a particle location, the known-vicinity algorithm outperforms all others Lohner (1995). Particle location at earlier time-steps provide a very good initial guess in LES. Knowing the initial and final location of the particle, this algorithm searches in the direction of the particle motion until it is relocated (Fig. 4). The neighbor-to-neighbor search is extremely efficient if the particle is located within 10-15 attempts, which is usually the case for 90% of the particles in present simulations. If this algorithm fails, we fall back to the 'modified-brute-force' method to locate the particle. A combination of these two algorithms is found highly efficient and robust for complex geometries and hybrid meshes encountered in realistic combustor geometries.

The known-vicinity algorithm is compared to the modified-brute-force method in Fig. 4. Two cases are considered: (i) domain size is fixed, and the particles are displaced for 2-3 cell-sizes in all three coordinate directions, (ii) the number of particles is kept fixed (1000 particles) and the element size per processor is increased. The known-vicinity approach is seen to be noticeably better than the modified-brute-force approach. Note that these comparisons were performed on a single processor of an Origin 2000.

Least-squares interpolation is used to interpolate gas-phase properties linearly each to particle location. Also particles that cross interprocessor boundaries are assigned to the ghost control volumes of the gas-phase solver, and then passed across processors.

4. Validation

The gas-phase solver was validated for a variety of benchmark flows: Taylor problem, isotropic turbulence, turbulent channel flow, flow over a cylinder, and the turbulent flow in a coaxial combustor. The simulations in the coaxial combustor geometry also included

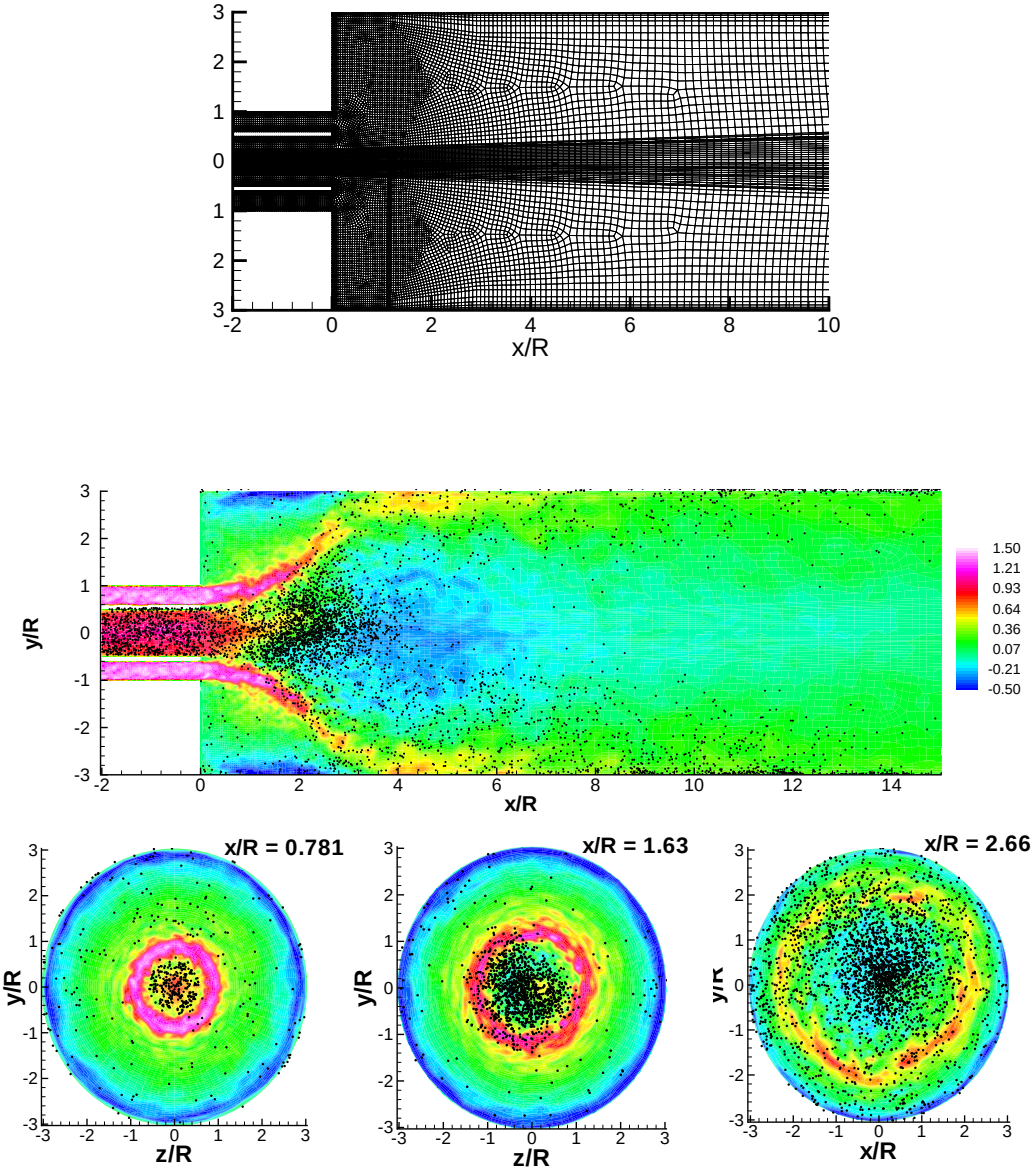

FIGURE 6. Cross-section of the grid and particles superposed on contours of instantaneous axial velocity in LES of the flow in a coaxial combustor geometry. Conditions correspond to an experiment by Sommerfeld & Qiu (1991). Only part of the computational domain is shown for clarity.

particles. The purpose of these validation studies was to establish that the algorithm can accurately simulate turbulence, is robust at high Reynolds numbers and on 'bad' grids, and has accuracy is comparable to that of structured grid solvers that use the same grid and computational stencil. Some of these validation cases are reported below.

Figure 5 shows results from computations of turbulent channel flow at $Re_\tau = 180$ on a very coarse grid ($32 \times 64 \times 32$). No subgrid model was used. Despite its simplicity, channel flow is known to be very sensitive to errors arising from the non-linear terms. On very

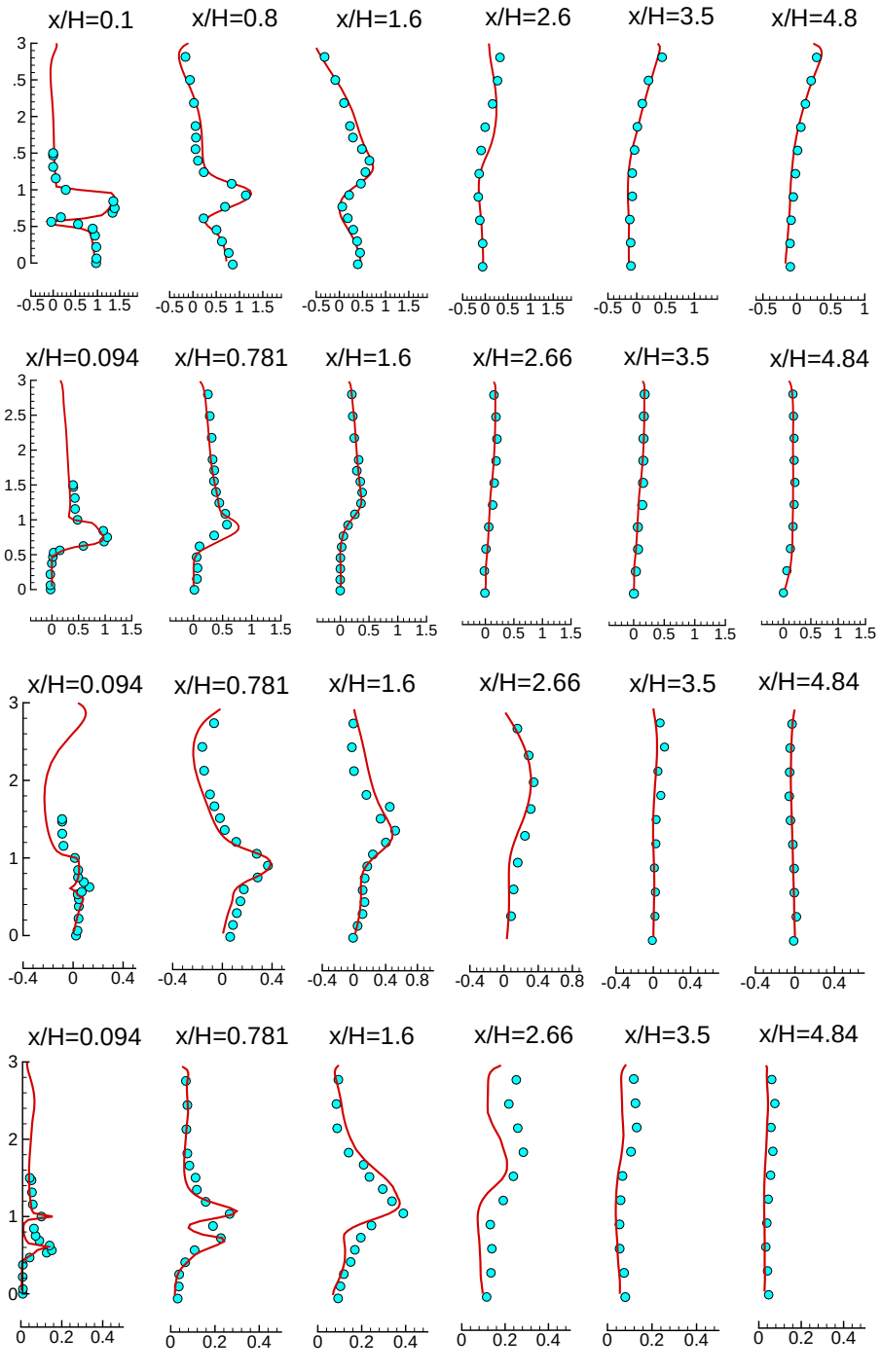

FIGURE 7. Comparison between LES (———) and experiment (○), Sommerfeld & Qiu (1991) for the gas-phase of particle-laden swirling flow in a coaxial combustor. (a): mean axial velocity, (b): mean swirl velocity, (c): mean radial velocity, (d) turbulent kinetic energy.

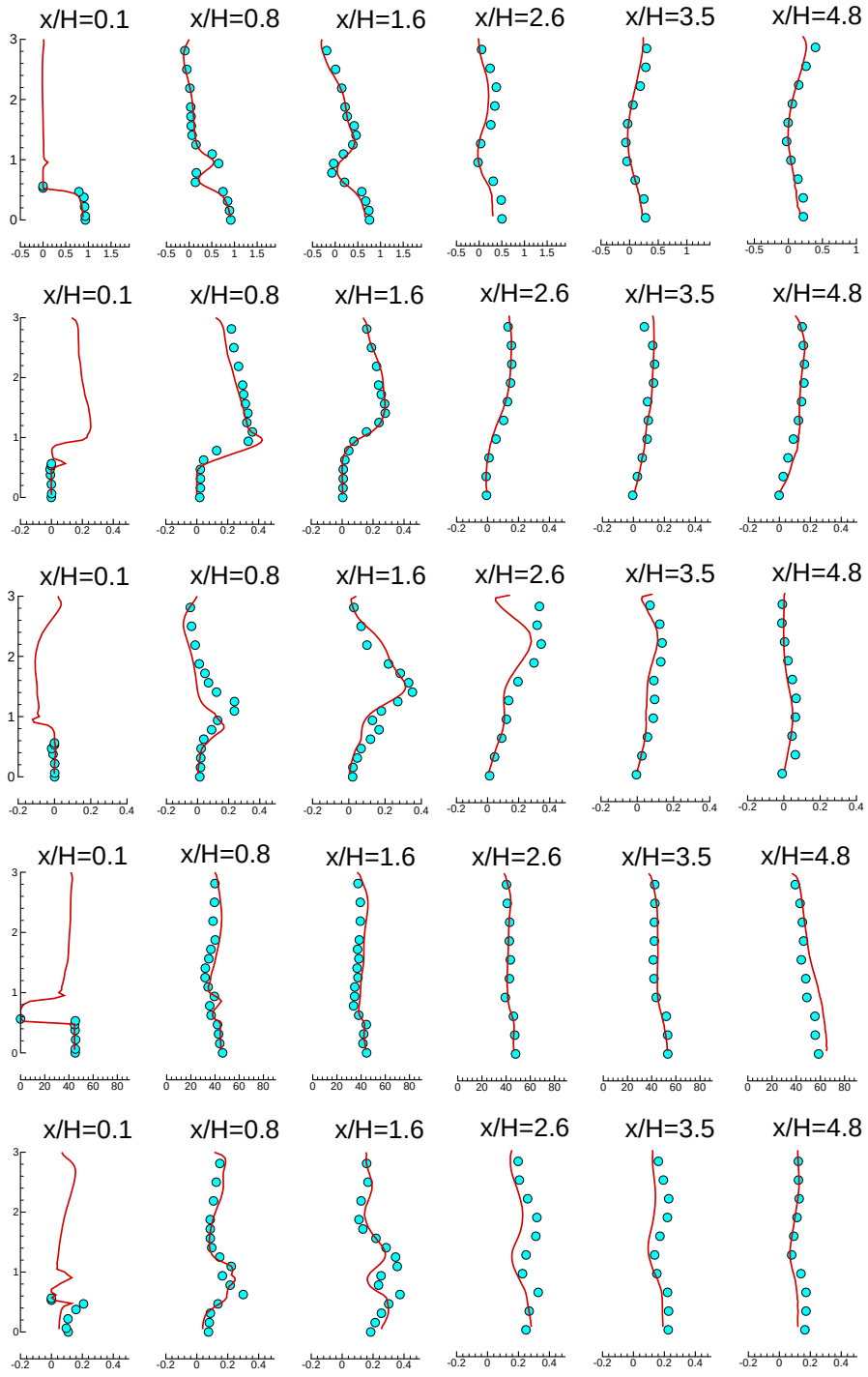

FIGURE 8. Comparison between LES (———) and experiment (○), Sommerfeld & Qiu (1991) for the particle-phase of swirling flow in a coaxial combustor. (*a*): mean particle axial velocity, (*b*): mean particle swirl velocity, (*c*): mean particle radial velocity, (*d*) mean particle diameter, (*e*) rms of particle axial velocity.

coarse grids, the turbulence in the channel can either decay or the entire solution can blow-up depending upon the numerical algorithm used. We compare our results to those provided by Dr. Bill Cabot (Lawrence Livermore National Laboratory) from a structured solver using the second-order staggered grid and fractional step approach on the same grid. The comparison shows that the accuracy of the unstructured algorithm is nearly the same as a structured solver for structured grids.

The flow in a swirl-stabilized coaxial combustor represents an important validation case. Sommerfeld & Qiu (1991) provide detailed measurements of this flow, which tests both the gas-phase solver and the spray module. A cross-section of the geometry and the unstructured mesh used for simulating this particle-laden flow is shown in Fig. 6. The flow is from left to right, and consists of a primary jet issuing out of the core, and a swirling jet issuing out of the annulus. The primary jet is laden with glass beads whose diameter varies from 20 microns to 80 microns. Detailed flow conditions and particle properties are summarized in Table 1. As a result of the swirl, the streamlines diverge as they exit into the dump region, and a recirculation region is set up (Fig. 6). The computations used an unstructured grid composed of approximately 2 million hexahedral elements. Turbulent fluctuations from a separate calculation are specified at the inflow and convective boundary conditions are imposed at the exit. The dynamic subgrid model was used. At the time of writing, flow statistics for the gas- and particle-phases have been computed. Figure 7 compares computed profiles of mean and turbulent gas-phase velocities with experiment, while Fig. 8 compares the corresponding particle statistics. In addition, variation of mean particle diameter is also compared. Good agreement is observed.

5. Simulations in Pratt & Whitney combustor

Validation calculations are being performed in the combustor of the PW6000 engine. These calculations are seen as a prerequisite to integrating the unstructured solver with the turbomachinery code. As shown in Fig. 9, the geometry of the PW6000 combustor is exceedingly complex, and poses serious challenges to both grid-generation and the solver. These simulations are being performed in two steps: (i) mixing of a passive scalar by cold flow (ii) introduction of heat release. The cold flow calculation is in progress, and results are reported below. Validation data is available for bulk quantities such as mass-splits and pressure drops for this case. Cold flow simulations are also being performed in a simpler configuration, termed the front-end validation model. This geometry has exactly the same fuel injector and combustion chamber as the PW6000 combustor, but is fed by a cylindrical plenum and does not have dilution holes (Fig. 13). It is being simulated because detailed LDV measurements are available from Pratt & Whitney. Note that the injector is the most geometrically complex component of the entire combustor. Quantitative validation for the front-end model will therefore establish considerable confidence in the results obtained for the PW6000 combustor.

5.1. *Grid generation*

A commercial grid generator (GAMBIT, Fluent Corporation) was used for grid generation. Both geometries (the PW6000 combustor and front-end validation model) were received from Pratt & Whitney as IGES files. The PW6000 geometry contained more than 9000 entities (surfaces, edges, vertices) which were cleaned up and reduced to 1200 entities. As shown in Fig. 9, the combustor chamber is fed by three coaxial swirlers and several dilution holes. The inlet air passes through the pre-diffuser and follows two

paths; the main stream flows through the swirlers and enters the chamber, while the secondary stream is diverted to the outer diffusers and enters the combustor through the dilution holes. Diversion of the outer diffuser air to secondary systems, and transpiration air through the liners of the main combustor, were not considered in the computations reported here; they are currently being included. The computational domain was divided into about 100 volumes for grid-generation; hexahedral meshes were generated over about 85% of the volumes. Tetrahedral meshes were generated for the swirlers, and pyramids were used to connect tetrahedral and hexahedral elements. An initial coarse grid has been generated; it contains about 1.3M elements (0.6M tetrahedra, 0.65M hexahedra). Figure 9 shows the grid. The level of geometrical complexity is obvious. Also note that the coarse grid consists of highly-skewed elements with rapid variations in element size and type. Figure 13 shows a schematic of the grid generated for the front-end validation model. The procedure described above was used to generate two grids: coarse (2.2M elements) and fine (4.5M elements).

5.2. *Results*

The flow conditions for the PW6000 combustor simulations are as follows. The flow into the pre-diffuser of the PW6000 is at a bulk Reynolds number of 500,000, which corresponds to a Reynolds number of approximately 150,000 in the main swirler, based on the diameter and flow rate through the swirler. Turbulent fluctuations from a separate computation in a pipe sector are specified at the inflow, and convective boundary conditions are specified at the exit. The flow in the domain was initialized to be at rest. Statistics were gathered after initial transients exited the domain.

The first computation performed in this geometry was at a very low Reynolds number of 1000, and did not include a subgrid model. Its objective was to assess the ability of the algorithm to handle a geometry with this level of complexity, and a mesh with extreme variations in size and element skewness. It was found that while geometrical complexity was adequately handled, 'bad' regions of the mesh posed severe problems. These problems were explained from energy-conservation principles, and the above-mentioned novel discretization was derived for the pressure gradient. This fundamental change in the algorithm has proven to be extremely successful in terms of its ability to handle complex geometries, high Reynolds numbers, and bad grids.

Figure 10 shows contour plots of both instantaneous and mean flow-fields in the PW6000 combustor. The flow in the diffuser is seen to be attached, it then passes smoothly through regions where the mesh rapidly changes, swirl is generated by the swirlers, and the flow in the dump region is determined by the interaction between the swirling primary jets and the dilution jets. Also shown in Fig. 11 are velocity contours from a computation on the same grid at the significantly lower inlet Reynolds number of 1000. No subgrid model was used in the low Reynolds number computations, while the high Reynolds number computations used the Smagorinsky model. The results at low Reynolds number are seen to be strikingly different, in that no recirculation region is seen downstream of the injector; instead the primary flow is jet-like. This behavior can be explained on physical grounds; the swirl that is generated by the swirler decays in the channel downstream of the swirler before the flow exits into the dump region. The decay rate of swirl is determined by the viscosity. At low Reynolds number, the decay of swirl

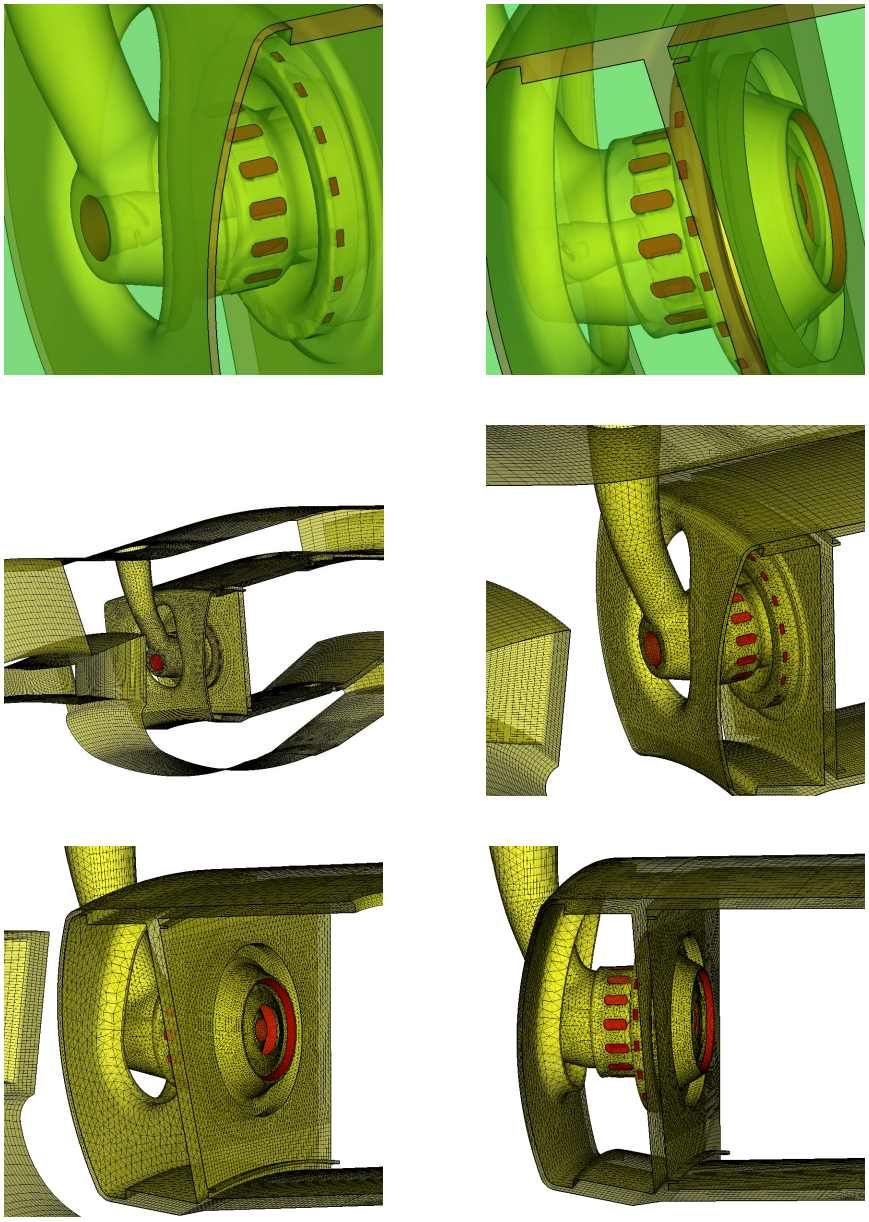

FIGURE 9. Illustration of the geometry and surface mesh in the PW6000 combustor geometry.

is significant enough that the exiting jet has negligible levels of swirl, and as a result no recirculation region is formed. On the other hand, at high Reynolds number the swirl velocity does not decay very much in the channel and, as a result, the exiting swirling jets diverge and a recirculation region is formed. This Reynolds-number sensitivity observed on a coarse grid is very encouraging, and reinforces the importance of having an algorithm that is robust without being dissipative.

The computations in the PW6000 geometry did not include the effect of outer-diffuser air being diverted to secondary systems, and transpiration air through the liner of the

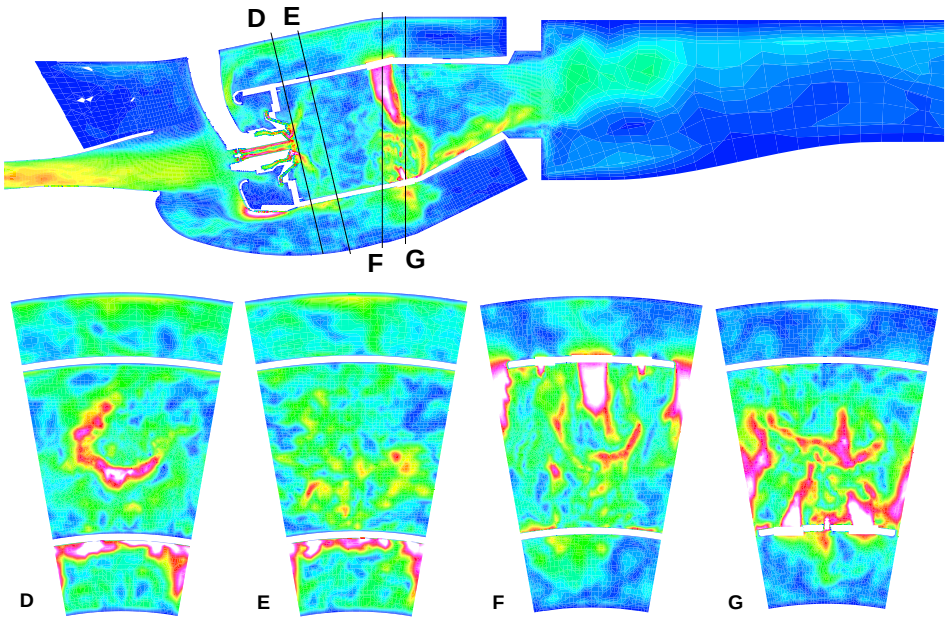

FIGURE 10. Contours of instantaneous velocity magnitude in LES of flow in the PW6000 combustor geometry.

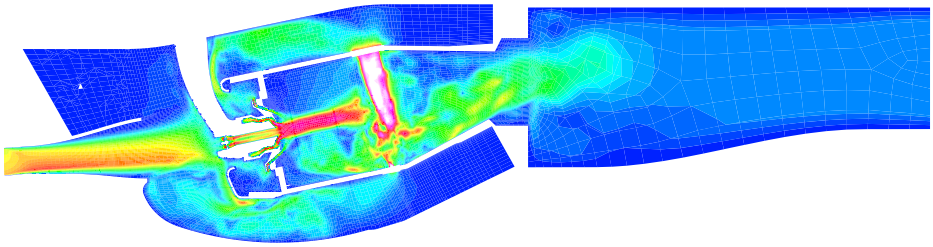

FIGURE 11. Contours of instantaneous velocity magnitude in the PW6000 combustor at a low inlet Reynolds number of 1000. Notice that flow downstream of the injector is jet-like instead of showing recirculation as in the high Reynolds number results shown above.

combustor. These effects have now been included, and a computation on the same grid is in progress. These results will be compared to bulk data like mass flow splits and mean pressure drops that will be made available by Pratt & Whitney. Also, computations are underway with particles; an instantaneous snapshot is shown in Fig. 12.

The front-end validation model is an important validation case because it uses the same injector as the PW6000 simulation. LDV data is available at three stations downstream of the injector. The Reynolds number in the main injector is approximately 100,000 in these computations. Figure 13 shows a schematic of the grid and contours of the velocity field. Two grids were generated: coarse (2.2M elements) and fine (4.5M elements). Simulations on the coarse grid have been performed, and used to initialize the fine grid computation which is underway. Statistics are being gathered on the fine grid at the time of writing. The mean pressure drop across the injector has converged, and shows very

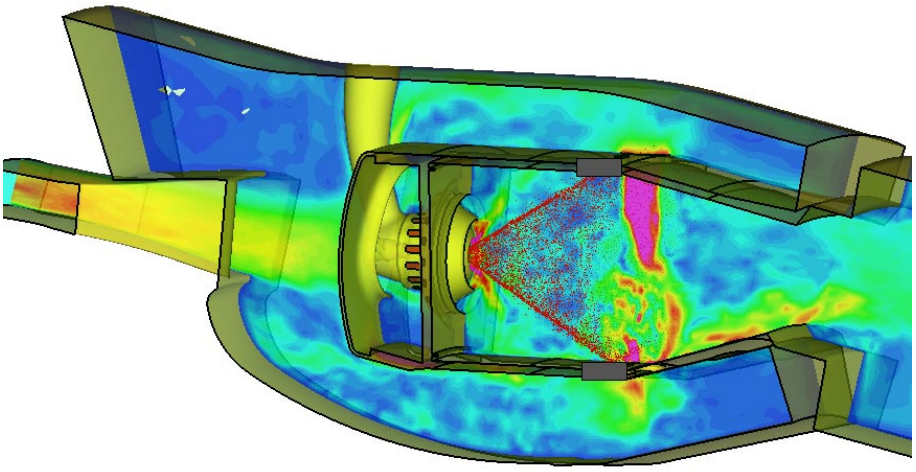

FIGURE 12. Instantaneous snapshot of particles superposed on velocity contours in PW6000 combustor geometry.

good agreement with experiment (4588 Pa as compared to 4500 Pa). In contrast, a RANS computation was performed on the same grid and found to yield a much higher drop of 5660 Pa. More detailed comparison will be performed once all quantities are converged.

6. Summary and future plans

Our progress in the last year is as follows:

• A new formulation was derived that is discretely energy-conserving for arbitrary grids. This was found essential for performing simulations at high Reynolds number simulations, and on the 'bad' grids found in complex geometries such as the Pratt & Whitney combustor.

• Turbulent validations were performed for the swirling flow in a coaxial combustor geometry, flow over a cylinder and turbulent channel flow.

• Turbulent simulations were initiated in the complex Pratt & Whitney combustor. Also, simulations were performed in a test rig geometry used by Pratt & Whitney for which experimental data is available.

• A spray module was integrated with the gas-phase solver. Validation simulations in a swiring coaxial combustor geometry Sommerfeld & Qiu (1991) were performed. Spray simulations in the Pratt & Whitney combustor were initiated.

Our plans for the next year are as follows:

• Complete validation in the front-end model.

• Complete validated simulations, including transpiration and secondary flows, in the PW6000 geometry.

• Perform reacting flow simulations in the PW6000 geometry.

• Extend the spray models to include droplet evaporation and spray-sheet break-up.

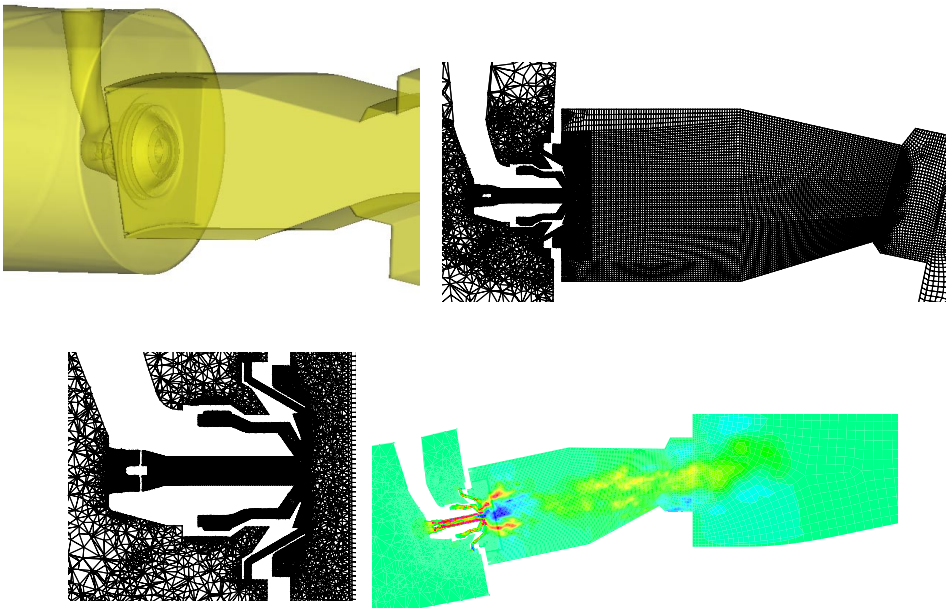

FIGURE 13. Illustration of the front-end validation model geometry, the grid, and instantaneous contours of streamwise velocity.

Acknowledgments

We would like to acknowledge Dr. Joseph C. Oefelein for his generous help in providing the spray modules developed for structured grids. Financial support for this work is provided by the Department of Energy's ASCI program.

REFERENCES

LOHNER, R. 1995 Robust, vectorized search algorithms for interpolation on unstructured grids. *J. Comp. Phys.* **101**, 307-313.

PIERCE, C. & MOIN, P. 2001 The progress variable approach for large eddy simulation of turbulent combustion. *Report TF-80*, Mech. Engg. Dept., Stanford Univ.

SOMMERFELD, M. & QIU, H. H. 1991 Detailed measurements in a swirling particulate two-phase flow by a phase-Doppler anemometer. *Int. J. Heat and Fluid Flow* **12**, 20-28.

WESTERMANN, T. 1992 Localization schemes in 2D boundary-fitted grids. *J. Comp. Phys.* **101**, 307-313.